fluids

MDPI

Article

On the Effect of Gas Content in Centrifugal Pump Operations with Non-Newtonian Slurries

Nicola Zanini *, Alessio Suman, Mattia Piovan and Michele Pinelli

Department of Engineering, University of Ferrara, Via Saragat 1, 44122 Ferrara, Italy
* Correspondence: nicola.zanini@unife.it

Abstract: Non-Newtonian fluids are widespread in industry, e.g., biomedical, food, and oil and gas, and their rheology plays a fundamental role in choosing the processing parameters. Centrifugal pumps are widely employed to ensure the displacement of a huge amount of fluids due to their robustness and reliability. Since the pump performance is usually provided by manufacturers only for water, the selection of a proper pump to handle non-Newtonian fluids may prove very tricky. On-field experiences in pump operations with non-Newtonian slurries report severe head and efficiency drops, especially in part-load operations, whose causes are still not fully understood. Several models are found in the literature to predict the performance of centrifugal pumps with this type of fluids, but a lack of reliability and generality emerges. In this work, an extensive experimental campaign is carried out with an on-purpose test bench to investigate the effect of non-Newtonian shear-thinning fluids on the performance of a small commercial centrifugal pump. A dedicated experimental campaign is conducted to study the causes of performance drops. The results allow to establish a relationship between head and efficiency drops with solid content in the mixture. Sudden performance drops and unstable operating points are detected in part-load operations and the most severe drops are detected with the higher kaolin content in the mixture. Performance drop investigation allows to ascribe performance drop to gas-locking phenomena. Finally, a critical analysis is proposed to relate the resulting performance with both fluids' rheology and the gas fraction trapped in the fluid. The results here presented can be useful for future numerical validation and predicting performance models.

Keywords: non-Newtonian fluid; centrifugal pump; kaolin slurries

Academic Editors: Chengcheng Tao and Mehrdad Massoudi

Received: 6 December 2024
Revised: 26 December 2024
Accepted: 7 January 2025
Published: 8 January 2025

Citation: Zanini, N.; Suman, A.; Piovan, M.; Pinelli, M. On the Effect of Gas Content in Centrifugal Pump Operations with Non-Newtonian Slurries. *Fluids* **2025**, *10*, 12. https://doi.org/10.3390/fluids10010012

1. Introduction

Centrifugal pumps are widespread consolidated machines to transport fluids in the industry thanks to their reliability and affordable price [1]. In certain fields, such as biomedical, food, and oil and gas, non-Newtonian fluids have to be managed [2–4]. Since the viscosity of a non-Newtonian fluid varies with the imposed stress and rheology, pumping this type of fluid can lead to a considerable variation in the pump performance, which is difficult to predict. In addition to pressure and temperature, the viscosity of a non-Newtonian fluid depends on the shear rate and usually is several orders of magnitude higher than water. Consequently, viscous effects cause a derating of pump performance with respect to water [5–7].

Previous experimental investigations with centrifugal pumps handling non-Newtonian fluids reported severe performance drops in part-load operations [5,8–10], whose cause is still not fully understood, and that can harm the plant's reliability and safety operations [3]. In addition, pump performance is usually provided by manufacturers only with water, and

thus also the selection process of the proper machine to handle non-Newtonian fluids may be very challenging. To overcome this problem, oversized pumps are commonly installed, increasing installation and operational costs [4]. In the literature, there are few models to predict the performance of centrifugal pumps with non-Newtonian fluids, and in these there is also a lack of reliability and generality [11,12]. Nowadays, pumping and mixing non-Newtonian fluids is a matter of increasing interest. In the last year, much progress has been made, but there is still a lack of detailed analysis of the fluid dynamics phenomenon inside these machines. Previous experimental results reported a strong dependence of pump performance on the type of fluid processed and the solid concentration in the mixtures [9,13]. Different detrimental phenomena are experienced throughout the operating range of the pump, and the most severe performance impairment is usually detected in part-load operations with high concentrated slurries [5]. Head and efficiency reductions up to −70% and −55% compared to the water baseline can even occur [14], compromising the safety of operations and leading to unexpected increase in operational costs. Such performance drops are ascribed to possible gas locking phenomena, but no concrete evidence has been provided so far [9,15,16]. In [15,16], head drops in part-load operations were also experienced, pumping phosphate clay slurries (shear-thinning fluids). Here, the air content in the processed slurries was reduced in an uncontrolled way, and the test in a de-aereated condition showed remarkable drop reductions. However, no quantitative or qualitative indication on the air content variation is provided.

This work aims to increase the knowledge of the instability phenomena that can occur when processing non-Newtonian fluids with centrifugal pumps. For this purpose, an extensive experimental investigation is carried out with an on-purpose test bench using kaolin mixtures as processing fluids. The choice of kaolin is mainly due to its ease of disposal, low environmental impact and with remarkable relevance in many industrial applications, e.g., paper, cosmetics, and paint industry [17]. In addition, kaolin slurries are well recognized as non-Newtonian fluids [18]. A small commercial centrifugal pump is here tested against three kaolin slurries at different solid concentrations, and rheological characterization is performed to outline fluid behavior. The influence of gas-locking phenomena in pump performance is investigated via a test in a standard or "industrial-like" condition, i.e., without altering the fluid after having prepared it, and in a "de-aerated" condition, that is, after removing air from the processed fluid. The air removal process occurs thanks to a vacuum pump connected directly to the test bench. The air removal effectiveness and the gas content in the mixture are qualitatively monitored with a bubble meter whose measuring principle is based on ultrasound. Tests in the "de-aerated" condition are compared with those in the standard one, and the resulting gap in performance is attributed to the entrained gas effect. Critical analysis is conducted to relate pump performance drops with the slurry's properties and the resulting performance.

2. Materials and Methods

The main characteristics of the experimental campaign with centrifugal pumps handling non-Newtonian fluids are described in this section. To evaluate the effect of NNF on pump performance, two kaolin slurries at various solid concentrations are considered. The fluid preparation procedure and the rheology characterization are also included. Finally, a strategy is established to investigate the detrimental effects in pump performance induced by gas-locking effects processing kaolin slurries.

2.1. Test Bench

Tests are carried out on an on-purpose test bench for pump performance designed and assembled at the Engineering Department of the University of Ferrara. The closed test

loop with a pressurizer described by Gülich [19] is taken as a reference for the design phase. A schematic representation of the test rig is reported in Figure 1.

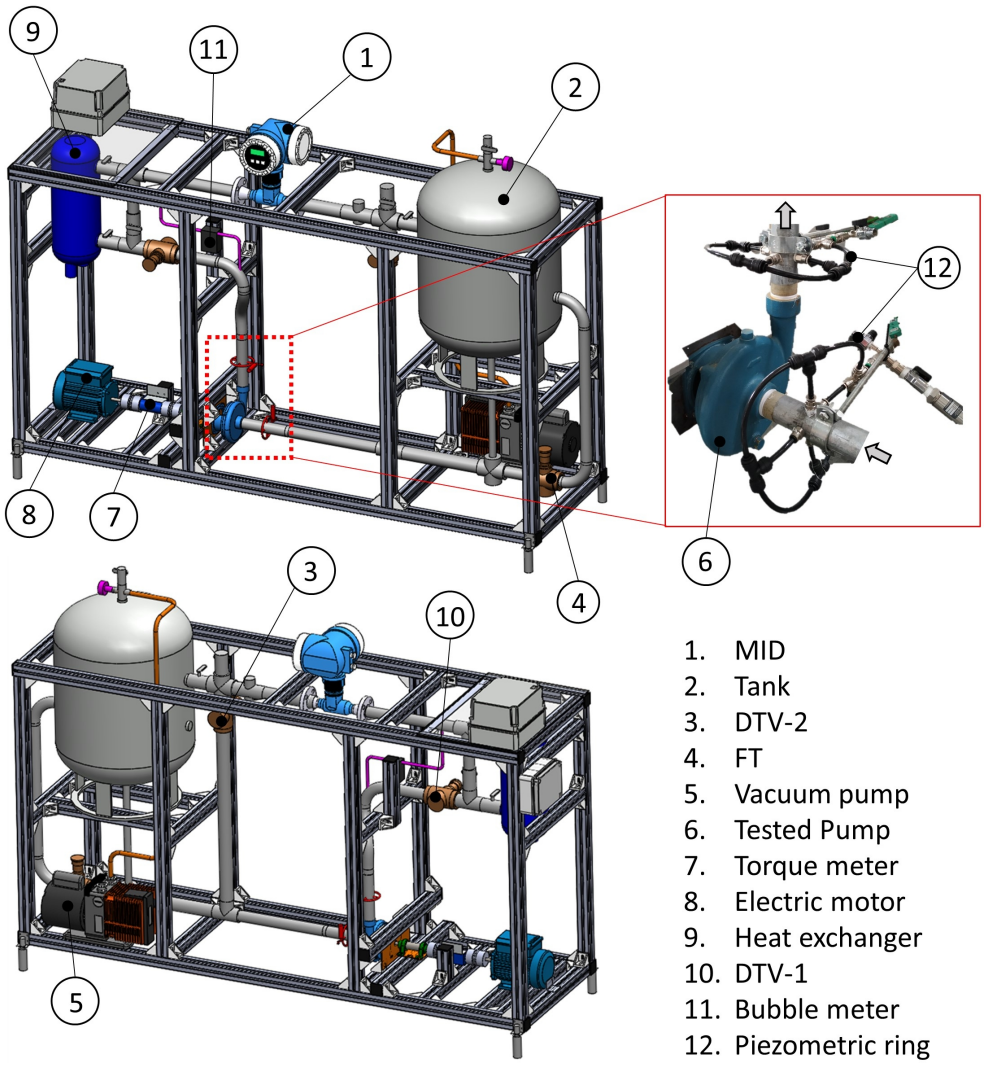

Figure 1. Test rig sketch.

The main loop is made up of 1 1/2″ galvanized steel pipes, 3.3 mm thick. A 100 L tank ensures the reservoir during the test. The constant fluid temperature during operations is guaranteed by means of a shell-and-tube heat exchanger (HE). The tested pump is actuated by a 1.1 kW inverter-driven electric motor (EM), and a Burster (Gernsbach, Germany) 8661-5005 torque meter (TM) is interposed between the motor shaft and the pump shaft. The rotational speed is measured with a magnetic pickup that overlooks the electric motor fan. The operational point of the pump is varied using a motorized throttle valve (DTV-1) and the volumetric flow rate is measured employing an electromagnetic flowmeter Endress+Hauser (Reinach, Switzerland) Proline Promag 55S (MID). According to the ISO 9906:2012 standard [20], the pressure measuring sections are located two diameters away from the suction and the discharge flanges. Each section is equipped with a K-type thermocouple and an absolute pressure transducer: a Measurement Specialties (Hampton, Virginia) pressure sensor U5131 (range of 0–2 bar) and a US381 (range 0–6 bar) are provided for the the suction and discharge section, respectively. The measured values of pressure and temperature are the average of four equally distributed taps joint by a piezometric ring, as reported in Figure 1. The pressure transducers are arranged horizontally to prevent the air and solid particles becoming trapped in the instrument lines. Another K-type

thermocouple and a Measurement Specialties Pressure sensor U5131 (range of 0–2 bar) monitor the fluid temperature and pressure in the tank. A pneumatic valve system at the top of the tank allows for the management of the pressurization of the test loop. The ambient pressure can be established by opening the vent valve while, utilizing a screw compressor and a vacuum pump, it is possible to pressurize or depressurize the loop. In addition, a SONOCHECK-ABD06 (Halle, Germany) bubble meter (BM) is installed next to the pump discharge section to evaluate the gas content inside the tested fluid. This non-invasive sensor is commonly employed for medical applications, e.g., to monitor the presence of bubbles during blood transfusions or dialysis by means of the ultrasound principle [21] or biotechnology processes [22]. The ultrasound wave emitted by the device crosses the measuring section (pipe), and depending on the transit time to reach the receptacle, an analog output is produced. Its signal is processed by internal algorithms, and it returns a signal proportional to the size of the bubbles detected. A branch from the main loop with a transparent plastic pipeline with an internal diameter of 4 mm is arranged to meet the installation requirements of the instrument. All signals from the measuring sensors and the control signals for the motorized valves are managed by an NI DAQ hardware system through software specifically developed in the LabVIEW (Austin, TX, USA) environment. Two different loop operative configurations can be alternately employed. In the "open-loop" scheme (Figure 2a), the DTV-2 is completely closed, and the fluid flows through the tank before reaching the pump suction. In the "closed-loop" scheme (Figure 2b), the tank is insulated by closing the FV and opening the DTV-2, and an additional vent valve is placed next to the MID. The closed-loop configuration is suggested to handle less volume fluid when no precise control of the internal pressure is required.

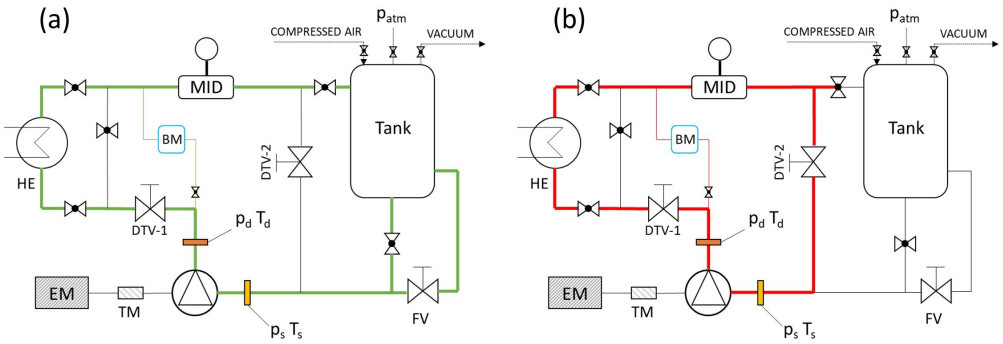

Figure 2. Loop configurations—(**a**) Open loop; (**b**) Closed loop.

2.2. Centrifugal Pump Tested

In this experimental investigation, a small commercial pump with a semi-open impeller is considered, whose depiction and main features are reported in Figure 3. The same pump was previously tested by the authors [13] with bentonite slurries, by Aldi et al. [10] and by Occari et al. [9] with kaolin slurries in a different test bench. The design speed is 2900 rpm and the performance at the best efficiency point with water returns a specific speed of 12.8. The impeller is 119.5 mm in diameter with seven blades. It is made of brass and the roughness is quantified in R_a = 3.15 µm with an Accretech (Tokyo, Japan) Handysruf$^+$ roughness meter. The clearance between the impeller and the casing can be varied freely in the test bench, and for the actual campaign it is set to 1 mm. The pump shaft is made of stainless steel while the seal is a composite carbon-ceramic-NBR. The operating limits can be summarized in a maximum allowable pressure of 6 bar and a fluid temperature in the range of −10 °C to 90 °C.

N [rpm]	2900
Q_{BEP} [l/s]	1.55
H_{BEP} [m]	18.5
n_q [rpm $m^{0.75}/s^{0.5}$]	12.8
D_{imp} [mm]	119.5
Z	7
Impeller axial clearance [mm]	1
R_a impeller [µm]	3.15

Figure 3. Centrifugal pump tested.

2.3. Fluids Tested

Kaolin comprises predominantly kaolinite, which is a soft mineral produced by the chemical weathering of aluminum silicate minerals like feldspar. Kaolin is one of the most versatile industrial materials, and consequently, its properties [23] and rheology [18] have long been studied. It is characterized by low reactivity to most of the industrial formulations over a relatively wide pH range, which accounts for many important applications [17]. Such characteristics as low surface charge, low surface area, white color, and particle shape make it a prime pigment and extender in paper coating and paints. One of the most important applications of kaolin is coating and filling paper. As a filler, kaolin is mixed with cellulose fibers in the wood pulp, and as a coating, kaolin is mixed with water, adhesives, and various additives and coated onto the surface of the paper. The shape and size distribution of kaolin powder are important factors in controlling many properties like brightness, viscosity, and ceramic strength and thus defining its intended application [24]. Kaolin concentration varies depending on the specific application, and it can reach 70 wt.%. Typical concentrations for the paper industry are between 30 wt.% and 40 wt.% [25]. Previous works [8,11] on performance prediction limit their analysis up to the 30 wt.% of kaolin concentration. This work extends the analysis of the non-Newtonian kaolin slurries handled by centrifugal pumps providing useful data for future analysis and developments on the pump performance modeling. A representative image with a scanning electron microscope (SEM) of the kaolin powder and the resulting Feret's diameter distribution are reported in Figure 4. The average particle diameter is 4.4 µm with a standard deviation of 3.1 µm.

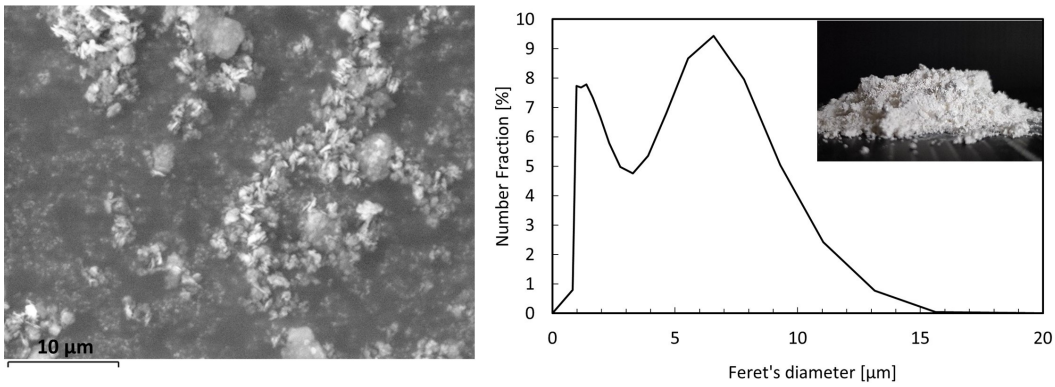

Figure 4. Kaolin SEM analysis.

2.4. Fluids Preparation

Kaolin slurries are prepared in a stirring tank separated by the test bench by mixing water and kaolin powder (Figure 4). For this experimental campaign, two solid concentrations for each type of slurry are considered, i.e., 35 wt.% and 40 wt.%. A total of 100 L

of tap water are mixed with a precise amount of powder to reach the required solid concentration. The mixture is kept under stirring to facilitate mixing for 8 h, and then it is left standstill. Time varies depending on solid content. For the most concentrated mixture, 24 h of standstill are sufficient, as suggested in [9,11]. Before filling the test bench, part of the fluid is spilled from the tank for the density and rheology characterization.

2.5. Fluid Characterization

Density and rheology measurements for the NNF are performed before the test campaign as follows. Density is obtained by weighing a measuring cylinder with a capacity of 100 mL filled with the fluid, and measurement uncertainty is estimated in ±0.5 mL. Measurements are performed with the Kern ABT 100-5NM analytical scale (Kern, Balingen, Germany), each measurement is repeated five times, and the resulting average value is recorded. Rheological data are obtained with rotational rheometer Rheometric Scientific ARES-LS equipped with 25 mm titanium parallel disks with a gap between the plates set to 1 mm. Rheology characterization is carried out for the range of shear rate between 1 and 500 s^{-1}, and the resulting apparent shear stress and viscosity are recorded. Experimental rheology data highlight the presence of non-zero yield stress and a monotonous decreasing viscosity increasing shear rate. According to [11,26], kaolin slurry behavior can be outlined using the Herschel–Bulkley model, which is suitable for shear-thinning fluids that exhibit yield stress at zero shear rate. The relation between shear stress τ and shear strain rate $\dot{\gamma}$ acting on the fluid assumes the following form:

$$\tau = \tau_0 + K\dot{\gamma}^n \quad (1)$$

where τ_0 is the yield stress, K is the consistency index, and n is the flow index. Three samples for each slurry are characterized and the average flow curve is considered. The estimated uncertainty of the reading value is quantified in ±2% for shear stress and ±3% for viscosity. The coefficients of the rheological models for each mixture are obtained from the best fitting of the experimental data using a nonlinear least-squares solver implemented in MATLAB R2023b. Finally, the resulting density and the model coefficients are summarized in Table 1 while the flow curves are reported in Figure 5. All the mixtures exhibit shear-thinning behavior ($n < 1$), and the higher the solid concentration, the steeper the flow curve obtained.

Table 1. Kaolin powder characteristic and slurry rheological model coefficients.

C_w [wt.%]	ρ_s [kg m^{-3}]	d_p [µm]	ρ [kg m^{-3}]	τ_0 [Pa]	K [Pa s^n]	n [-]
35	2800	4.5	1207	0.596	6.750	0.2176
40	2800	4.5	1238	3.082	9.670	0.2628

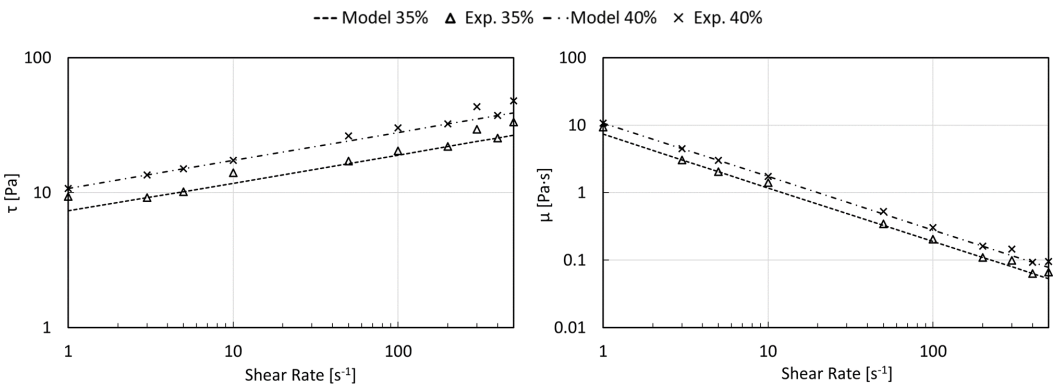

Figure 5. Kaolin rheology characterization.

2.6. Test Methodology

The influence of possible trapped air on pump performance is investigated through tests with reduced air content in the fluid. For this purpose, this procedure is performed here with the kaolin slurries since they demonstrated good affinity in incorporating air in previous experimental investigations [9,15]. The pump performance with water and the two kaolin slurries are investigated across the operating range of the pump. The flow rate is varied by setting the position of the motorized globe valve located next to the discharge section DTV-1 (Figure 1). Preliminary tests do not report any hysteresis of the flow rate moving from full load to the pump shutoff or vice versa. The instruments and the acquisition system are switched on thirty minutes before starting the test to check the stability of the signals. Then, the test bench is filled with the selected fluid and the pump is kept running for fifteen minutes before starting the recordings. The entire operating range is divided into twenty equally distributed points and the measurements are taken starting from the full-load condition. Fewer points are considered when the high viscosity of NNFs prevents them from reaching at least the water's best efficiency point. The measuring process starts by fully opening the motorized valve. Once the stability of the signals is reached, the measurements are recorded every second for one minute and the resulting average and standard deviation are registered. Then, the process is repeated for all the other points with the same strategy. Once the performance test is completed, a strategy is set up to remove air from the fluid using a vacuum pump that extracts air from the top of the tank as follows. The vent valve of the test bench is closed and the pump is kept running at a low speed, i.e., 500 rpm, to ensure the air removal from the entire mass of fluid in the bench and at the same time to prevent excessive shaking of the mixture and thus the re-entrainment of air. The degree of air is controlled by means of a bubble meter whose signal intensity is proportional to the gas content of the fluid. According to the manufacturer's specifications, the output is in the range of 0–250, where 0 corresponds to the full pipe (zero gas fraction) and 250 is the empty pipe condition. The starting air level in the fluid is acquired before running the vacuum pump and then the signal is monitored during the air extraction. The average output value decreases over time when the vacuum pump is on and the process ends when the signal becomes stable. Preliminary tests report that approximately thirty minutes are adequate to conclude the air removal process. The bubble meter signal trend during air extraction is schematized in Figure 6. Finally, the pump performance test in reduced air content conditions is carried out following the same strategy proposed for the reference condition, i.e., from full load to the pump shut-off.

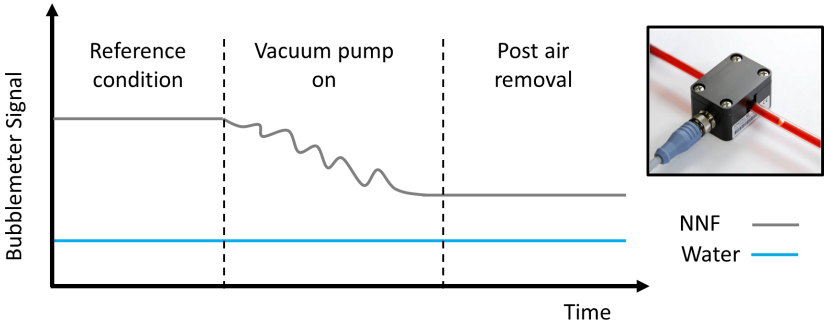

Figure 6. Bubble meter signal trend during the air extraction process.

3. Results

The resulting pump performance with water and non-Newtonian fluids for three pump speeds, i.e., 2000 rpm, 2500 rpm, and 2900 rpm, are presented. Pump performance in de-aerated and standard conditions, i.e., before the air removal process, for the non-Newtonian fluids are also included in the analysis and discussed. Pump performance is

commonly evaluated in terms of pump total head (H), shaft power (P_s), and efficiency (η) as follows:

$$H = \frac{p_d - p_s}{\rho g} + \frac{v_d^2 - v_s^2}{2g} + (z_d - z_s) \tag{2}$$

$$P_s = C\Omega \tag{3}$$

$$\eta = \frac{\rho Q g H}{P_s} \tag{4}$$

where p_d and p_s are the static pressures at the pump discharge and suction, respectively, ρ is fluid density, z_d and z_s are the heights of the measuring sections at the pump discharge and suction, Q is the volumetric flow rate, Ω is the pump angular speed, C is the mechanical torque, v_d and v_s are the fluid velocity at the pump discharge and suction. Since the suction and the discharge nozzles have the same diameter, the velocity head cancels.

3.1. Measurement Uncertainty

The uncertainty quantification is essential for any experimental campaign in order to estimate the confidence band and the quality of a set of measurements. Here, the uncertainty of each performance parameter is calculated based on the instruments' datasheet and on the relevant regulatory standards. An uncertainty calculation based on the procedure reported in the standard ISO/IEC Guide 98-3:2008 [27] and EA-4/02M [28] is performed in order to estimate the uncertainty of the pressure measurements. The two pressure transducers and the correspondent measurement chain are calibrated at the same time, employing pressure calibrator MicroCal PM200+ representing the in-house laboratory secondary standard which, in turn, is calibrated towards a primary laboratory standard certified in agreement with the Italian Accreditation Body (Accredia). Type B uncertainty is obtained by considering the uncertainty of the primary laboratory standard as reference uncertainty U_{PLS} and the residual uncertainty value of the pressure measurement chain E_R. The former (U_{PLS}) is the supposed Gaussian distribution, and consequently it is divided by two for calculating the standard deviation equivalents, while the latter (E_R) is estimated considering the difference between the reference value (also called the true value) and the average value of the signal provided by the measurement chain reordered for 10 s under a constant pressure input (generated and controlled by MicroCal PM200+). This term is considered to have a rectangular probability distribution, and for this reason, it is divided by $3^{1/2}$. Finally, the evaluation of Type A uncertainty is carried out by estimating the standard deviation (considered as a Gaussian distribution, and for this reason, it is divided by two for calculating the standard deviation) of the data set U_σ. The final assessment of the pressure measurement uncertainty is performed in Equation (5).

$$\delta p = \sqrt{\left(\frac{U_{PLS}}{2}\right)^2 + \left(\frac{E_R}{\sqrt{3}}\right)^2 + \left(\frac{U_\sigma}{2}\right)^2} \tag{5}$$

The uncertainty of the other instruments is derived from the corresponding datasheet. The uncertainty of the flow meter (Endress+Hauser Proline Promag 55S) is equal to ± 0.2 %R and the combination of relative non-linearity, hysteresis, and sensitivity returns an uncertainty for the torque meter (BURSTER 8661-5005), amounting to ± 0.015 N. The pump speed uncertainty is estimated at ± 10 rpm. The propagation of uncertainty is realized according to ISO/IEC Guide 98-3:2008 [27], which allows calculating the extended uncertainty u_c for a given variable y as follows:

$$u_c(y) = \sqrt{\sum_{i=1}^{N} \left(\frac{df}{dx_i}\right)^2 u^2(x_i)} \tag{6}$$

where x_i are the dependent variables of the f function, which define the variable y, and $u(x_i)$ is the uncertainty related to each dependent variable evaluated like for the pressure measurements in Equation (5). This procedure is followed to calculate the extended uncertainty for the pump head and efficiency, which are estimated to be, respectively, ± 0.23 m and $\pm 1.5\%$.

3.2. Water Test

Test with water constitutes the reference pump performance and the results are reported in dimensional coordinates. Similarity operating conditions with water at different pump speeds are verified using typical dimensionless parameters. By the procedure of dimensional analysis using Buckingham's theorem and the three primary dimensions, mass, length, and time, it is possible to form dimensionless groups. The dimensionless groups for volume flow rate and pump head according to [1], i.e., the flow coefficient ϕ and the head coefficient Ψ, are here considered:

$$\phi = \frac{Q}{\Omega D_2^3} \tag{7}$$

$$\Psi = \frac{gH}{\Omega^2 D_2^2} \tag{8}$$

Meanwhile, specific speed is calculated according to Equation (9):

$$n_q = N \frac{\sqrt{Q_{BEP}}}{(H_{BEP})^{0.75}} \tag{9}$$

The resulting performance with water is depicted in Figure 7 and the performance at the best efficiency point for each pump speed is summarized in Table 2.

At nominal speed (2900 rpm), the maximum efficiency achieved is 50.6% and the specific speed is 12.7, which is a conventional value for radial pumps, as reported by Gülich [1]. When decreasing the pump speed, the maximum efficiency drops almost linearly up to the 36.2% for a test at 2000 rpm. Finally, affinity laws are employed to verify the similarity of operations at different pump speeds by plotting the head coefficient Ψ against the flow coefficient Φ, as depicted in Figure 8. The similarity is considered verified since the maximum deviation obtained is at most 5% for all the operating ranges of the machines. Higher deviations are found only for a few operating points at $\phi > 0.003$, where the maximum uncertainty reaches 8%.

Table 2. Performance at the best efficiency point with water at various pump speeds.

N [rpm]	Q_{BEP} [L/s]	H_{BEP} [m]	P_s [W]	η [%]	n_q
2900	1.54	18.71	557.8	50.6	12.7
2500	1.18	13.00	319.0	47.1	12.6
2000	0.76	6.67	137.8	36.2	13.3

3.3. Kaolin Test

Pump performance derating while handling NNFs is evaluated by comparing the water baseline with the corresponding slurry performance. The results are presented using dimensionless coordinates (q^*, h^*, p_s^*), which are, respectively, the flow rate, the pump head, and the shaft power reduced with respect to the performance obtained at the best efficiency point with water (BEP_w) for a given rotational speed:

$$q^* = \frac{Q}{Q_{BEP_w}} \qquad h^* = \frac{H}{H_{BEP_w}} \qquad P_s^* = \frac{P_s}{P_{s_{BEP_w}}} \tag{10}$$

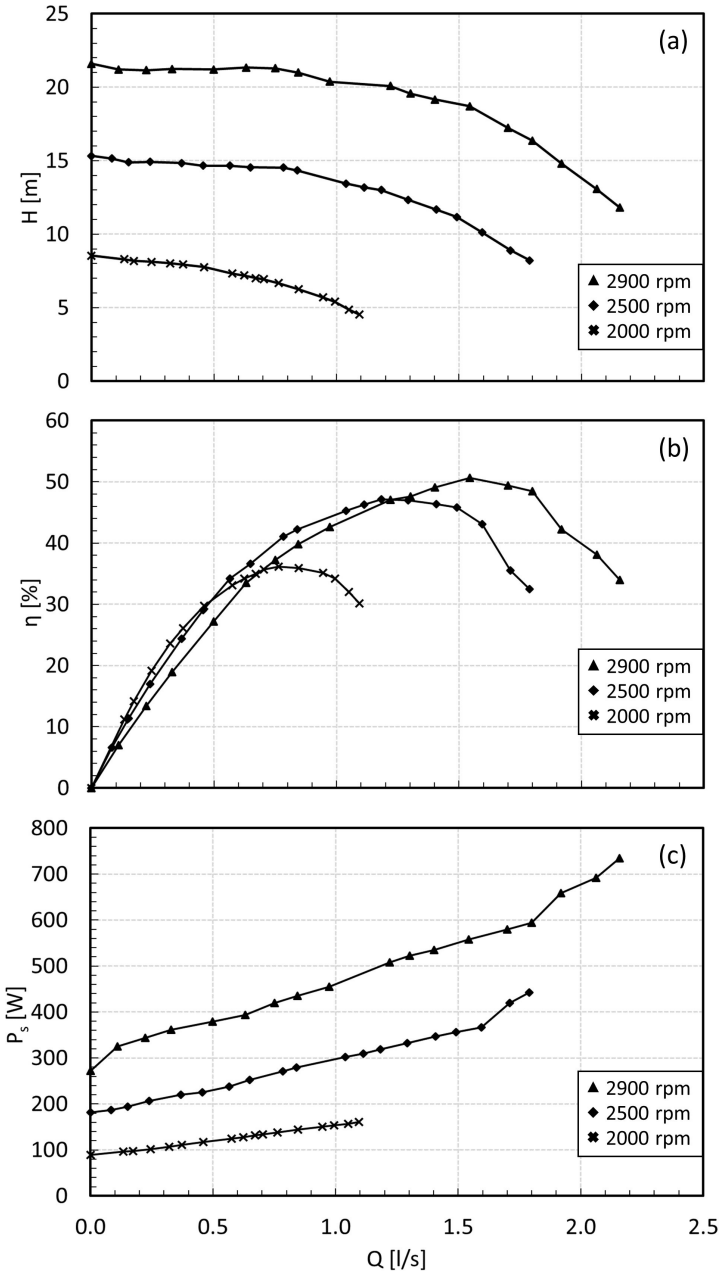

Figure 7. Pump performance with water—(**a**) Pump Head, (**b**) Efficiency, and (**c**) Shaft power.

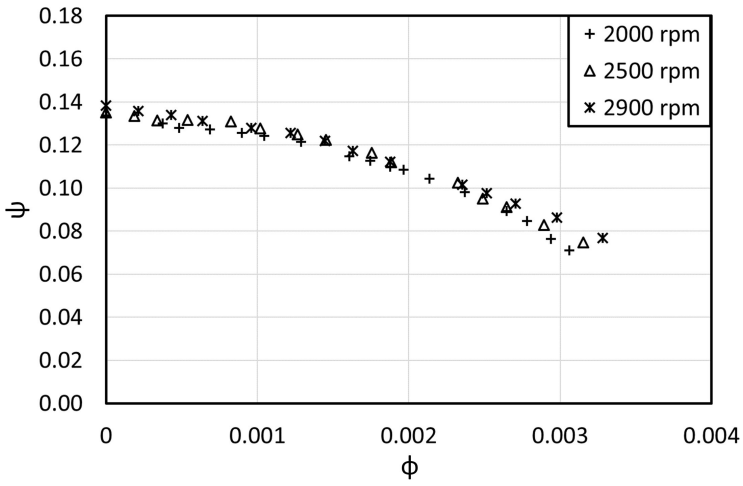

Figure 8. Water performance in dimensionless coordinates.

Pump efficiency is reported as calculated (Equation (4)) to avoid misunderstandings in scaling an already dimensionless number. A summary of the resulting derating coefficients is also proposed to highlight the performance modification trend according to each type of NNF tested. In addition, suction and discharge pressures in dimensionless form (reduced as Equation (10)) are employed to carry out the analysis on the gas-locking effects on pump performance. For greater clarity of the result graphs, the extended measurement uncertainty is included in the marker's width. Two solid concentrations of kaolin slurries are tested at three rotational speeds: 2900 rpm (design speed), 2500 rpm, and 2000 rpm, and the resulting performance is acquired in the standard condition first. Tests at reduced speed were carried out to investigate the sensitivity of pump performance and operating conditions to reduced speeds. Once performance in the standard condition is acquired, an air removal process is established to reduce the gas content in the fluid. As described in Section 2.6, the effectiveness of the air removal process is evaluated by means of a bubble meter. According to the manufacturer's specifications, quantitative information about the gas fraction can be derived only for pure water because the presence of suspended particles in non-settling slurries can widely influence the scattering of the ultrasound wave. Consequently, the signal with NNFs contains both bubble and suspended particle disturbances. To overcome this problem, the bubble meter is here employed only for comparative analysis among water and NNFs in both standard and de-aerated conditions. In addition, the bubble meter is used to determine the end of the air extraction process as follows: (i) the average signal in the standard condition is acquired and registered; (ii) the air removal process begins and the bubble meter signal decreases while the air is being extracted; (iii) the air removal process ends when the signal becomes stable at a lower value than the reference one. This means that the air has been removed as much as possible and the scattering contribution due to the bubbles is eliminated, or at least reduced to minimum. In Figure 9a, a comparison of the obtained signals acquired for 60 s for pure water (reference) and the 40 wt.% slurry in both standard and de-aerated conditions is reported.

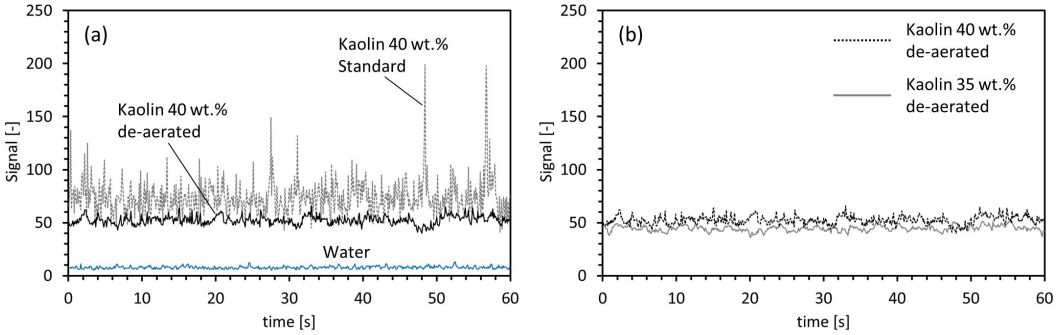

Figure 9. Bubble meter signal—(**a**) water signal (blue line) compared with kaolin 40 wt.% in standard and de-aerated conditions; (**b**) de-aerated mixtures, 40 wt.% vs. 35 wt.%

Looking at the slurry in the standard condition, it appears clear that the combined presence of gas and solid particles leads to a higher average signal compared to the reference and also larger signal fluctuations. Focusing on the de-aerated slurry instead, both the average signal and the fluctuations are severely reduced due to the lesser air content in the mixture. To reach this condition with the actual setup of the test bench, thirty minutes of air extraction are needed for a 40 wt.% or twenty minutes for the lighter slurry (35 wt.%). Figure 9b instead compares the 35 wt.% and the 40 wt.% slurries in the de-aerated condition, always for an acquisition time of 60 s. Slight differences can be outlined from these trends, but it is evident that for the lighter slurry (35 wt.%), the average signal is lower than for the heavier one (40 wt.%) due to the reduced solid content, which is physically coherent with

the measurement principle. Once the de-aerated condition is established, performance tests are carried out. Finally, the performance in standard and de-aerated conditions is depicted in Figure 10.

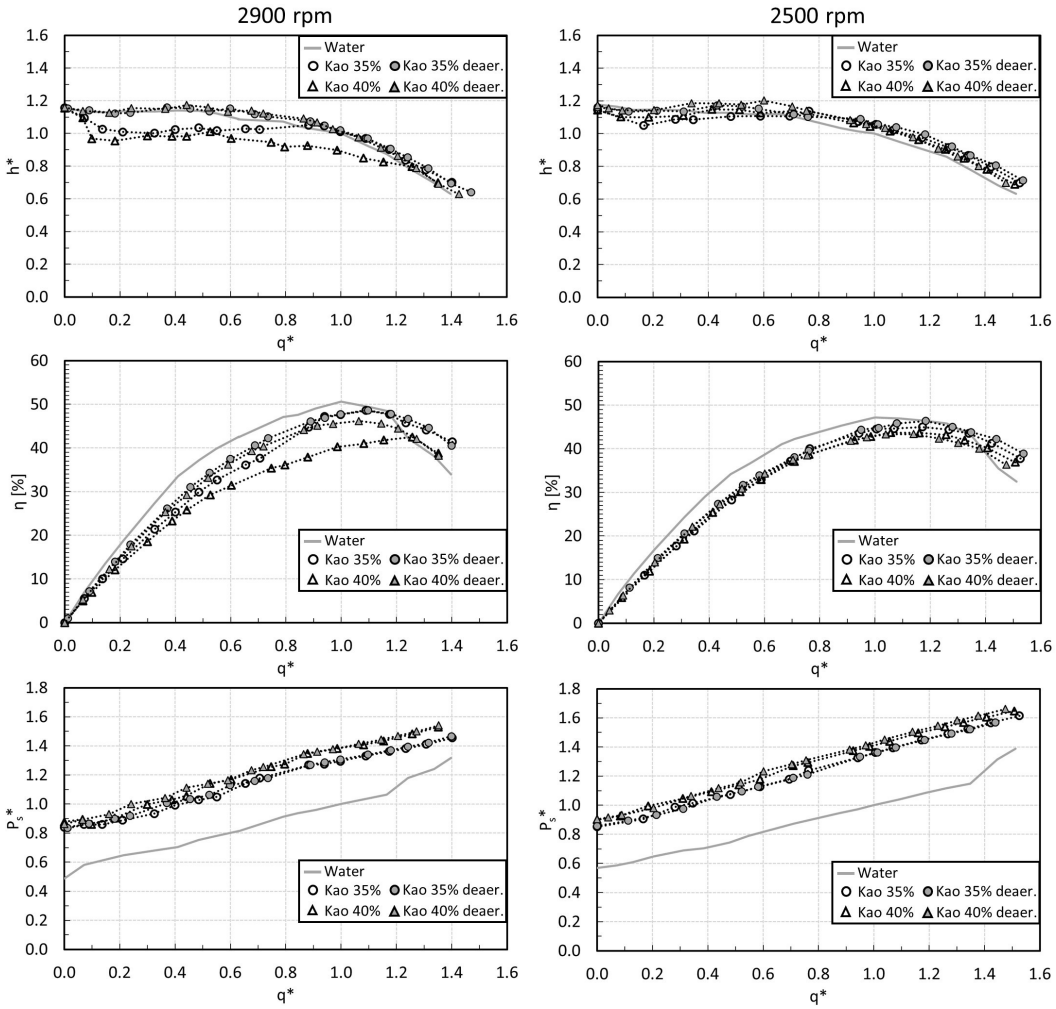

Figure 10. Pump performance with kaolin slurries—2900 rpm and 2500 rpm.

4. Discussion

4.1. Kaolin Performance in Standard Condition

It appears clear how the pump head with kaolin mixtures overcomes the water one in overload operations for all the tested speeds. This phenomenon, called the sudden-rising-head effect, was previously experienced by several authors in the literature [10,29,30], and it can occur when handling Newtonian fluids slightly more viscous than water. In this condition, both head and efficiency exceed the performance with water for all the tested mixtures. The efficiency with the viscous fluids at 2000 rpm and 2500 rpm reports an increment of up to 5% of the efficiency with water at high flow rates. This result is in line with the outcomes of [10,30]. The efficiency improvement due to the sudden-rising-head effect increases with q*. The viscous head is found to be 8% higher than the water one at q* = 1.37 with 35 wt.% but negligible with 40 wt.% slurry. Typical head drops detected in part-load operations while processing non-Newtonian fluids are also experienced. The entity of the maximum head drop appears dependent on both the solid content and the pump speed. Generally, the higher the solid content, the greater the head drop obtained at part load for a given rotational speed. At the same time, operating close to BEP and in overload, the pump heads with both kaolin slurries are practically identical, thus indicating the independence of the head from solid content in such conditions. For example, a test

at 2000 rpm (Figure 11) at the higher flow rates reported that the kaolin head overcame the water one and no remarkable differences were found processing 35 wt.% or 40 wt.%. The maximum head deviation for q* > 1 results in less than 1%. Moving to lower flow rates, the viscous pump head drops below the water without recovering while reducing the flow rate. The flow rate for which the drop is experienced varies with the solid content, i.e., the more concentrated the mixture, the higher the flow rate that determines the beginning of the drop. In addition, increasing the solid content in the mixtures involves higher deviations of the pump head at low flow. A test at 2000 rpm reported a maximum deviation of 15% between the 35 wt.% and the 40 wt.% slurries at around q* = 0.2. Increasing pump speed (2500 and 2900 rpm), a similar trend for the head is outlined: the heavier the mixture, the higher the flow rate for which the viscous head drops below the water one, and the larger the instability in part-load operations. A test at 2500 rpm showed a viscous head slump that starts from q* = 0.9 and reaches a maximum gap with water up to 12%, while for the test at 2900 rpm, the drop starts at around q* = 1.2 and reaches a maximum of 15% of deviation from water. Shaft power and pump efficiency vary significantly when processing kaolin slurries instead of water and, at the same time, they appear less affected by the solid content in the mixture than the pump head. The highest shaft power in each test condition is obtained with the 40 wt.% mixture and, compared to water, it is found increasing from 38% to 45%. In parallel, shaft power with the 35 wt.% slurry differs only up to 8% less than the heavier mixture. In particular, for 2000 rpm tests it is difficult to notice noteworthy differences throughout the operating range. Always in the tests at 2000 rpm, the greatest increase in power is found processing viscous fluids and is quantified in +45% at q* = 1. Pump efficiency follows a similar trend. Generally, processing kaolin slurries entails remarkable efficiency reductions whose entity is dependent on the solid content, and the higher the pump speed, the more sensitivity to solid content in the mixture. Comparing the performance at 2500 rpm and 2900 rpm, it can be noted that the lowest efficiency is always obtained with the heavier slurry (40 wt.%) and that at high speed (2900 rpm), the slurry efficiency curves differ more than at low speed (2500 rpm). It is also observed that this deviation is clearer near the water BEP (q* = 1) and that at the highest flow rates, the viscous efficiency can also overcome the water one. In part-load operations, instead, pump efficiency appears independent of the solid content. The best efficiency point with kaolin slurries moves to higher flow rates compared to water. Paternost et al. [31] stated that the presence of large bubbles at the pump intake can greatly affect pump performance; in addition, coalescence played an important role in head modification. Large bubbles tend to stagnate at the pump impeller, leading to surging conditions. For a given gas fraction, higher liquid viscosities impact the pump performance greatly. Fewer bubble breakups occur due to lower turbulence, and consequently, large bubbles might be formed. It appears clear that processing kaolin slurries can involve remarkable variations in expected pump performance. First of all, the shape of the pump head curve demonstrates that unstable operating points can be established at part load, where the derivative of the performance curve becomes positive and unexpected head drops occur. The magnitude of such drops appear directly dependent on the solid content in the mixture. In this light, the lack of the required (or expected) head could involve operational issues, safety risks, and unplanned production shutdowns. On the other hand, the increasing power required could involve high and difficult to predict process costs.

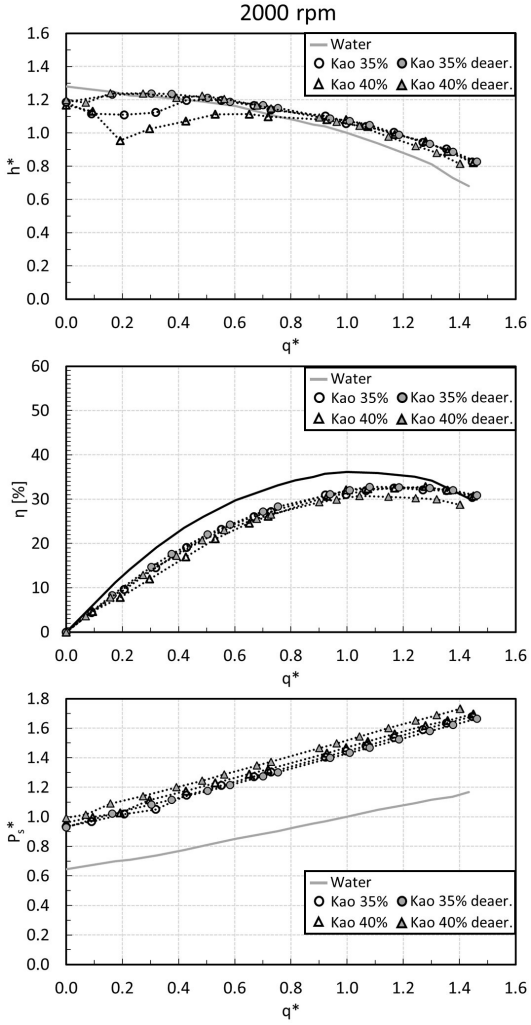

Figure 11. Pump performance with kaolin slurries—2000 rpm.

4.2. Kaolin Performance in De-Aerated Condition

It appears clear that the presence of air bubbles in the fluid strongly influences pump performance. For both mixtures, the standard tests report severe head drops to obtain unstable operating conditions, especially in part-load operations. Shaft power increases up to +45% compared to water and pump efficiency, resulting in remarkably reduced processing of kaolin slurries. Overall, higher kaolin concentrations correspond to greater drops, and increasing rotational speeds leads to extending the unstable curve to higher flow rates. Looking at the de-aerated results, the air removal process seems to alter significantly the characteristics of the slurry. The de-aerated tests show no head instabilities at all flow rates, resembling Newtonian water-like behavior for both speeds. At the highest flow rates, where the sudden-rising-head effect is established, no remarkable difference between standard and de-aerated tests is found. In this way, the greatest influence of the trapped gas occurs at part load, where higher deviations between standard and de-aerated tests are found. Here, pump head is recovered up to the +20% of the water head between q^* = 0.2 and q^* 0.5. At the highest flow rates, instead, the presence of gas could be substantially neglected. This behavior could be ascribed to the combination of two main effects while reducing flow rate: (i) higher pressure difference across the pump and (ii) lower flow rate, i.e., lower capacity to drain the impeller passages from gas accumulation. The difference in density between the liquid and gas phases allows the bubbles to move easily upstream and thus follow the adverse pressure gradient [32]. Consequently, operating at low flow rates involves a higher probability of bubble stagnation inside the impeller. The suction

and discharge pressure over the pump operating range are also analyzed. To facilitate comparison with the water tests, the pressures are dimensionless with respect to the pressure obtained at BEP with water:

$$p_s^* = \frac{p_s}{p_{s_{BEP_w}}} \qquad p_d^* = \frac{p_d}{p_{d_{BEP_w}}} \tag{11}$$

The resulting dimensionless suction and discharge pressures are reported in Figure 12. Experimental data report that the discharge pressure trend follows the head one, so the drops at low flow rates could be ascribed to the compressibility effects introduced by the air bubbles that change their characteristics (density and thus the occupied volume) over the pump. The compressibility effects due to the presence of air bubbles within the fluid generate a modification of the pressure value at the pump discharge section (see Figure 12a–c), while the suction pressure seems not to be affected by the air content (see Figure 12d–f). At the same time, comparing the different rotational speeds, this phenomenon is not triggered in a non-trivial way by the pressure, but it is a combination of the pump operating point (i.e., rotational velocity and flow rate) and fluid characteristics (i.e., solid particles and air bubble content).

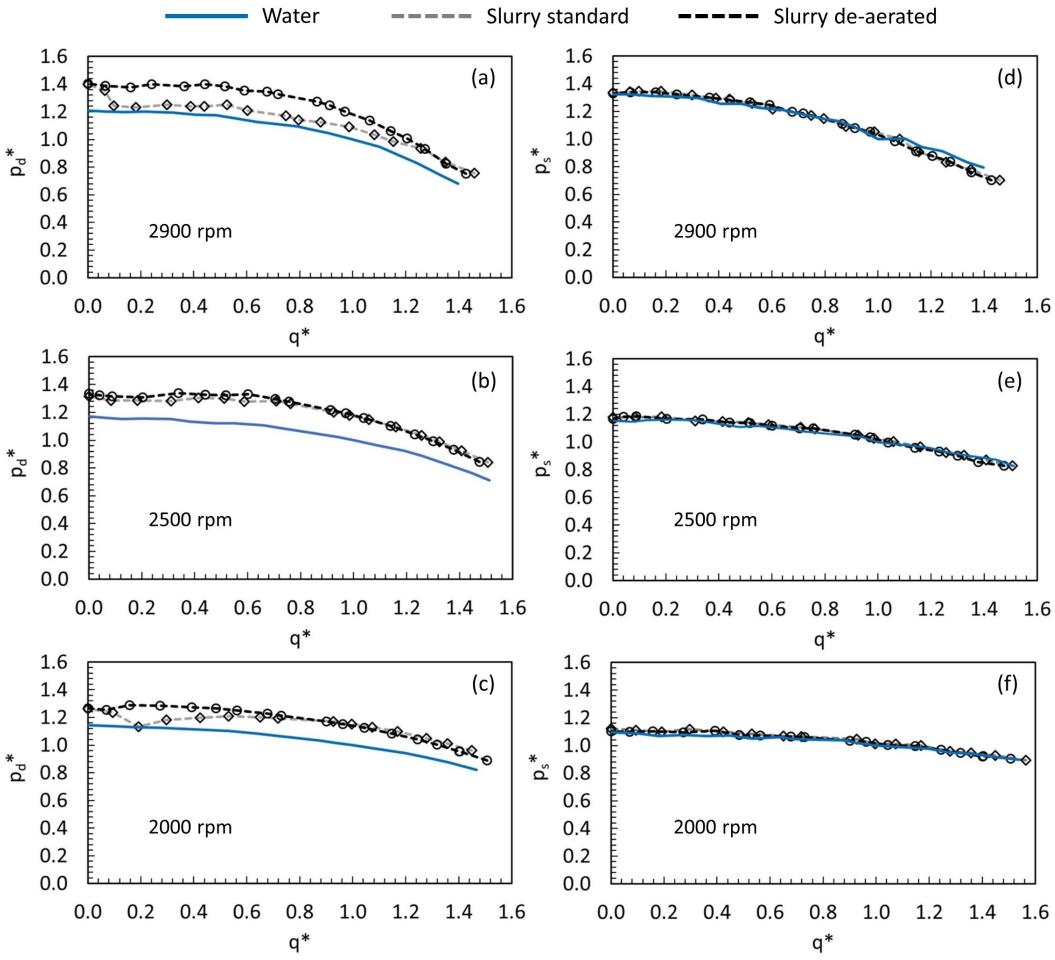

Figure 12. Dimensionless discharge pressure p_d* (**a–c**) and suction pressure p_s* (**d–f**) testing kaolin slurries.

The effect of free gas in water was extensively studied in [33] for different gas volume fractions, where the same type of instability observed in the present study was detected. Pump efficiency also increases when the mixture is de-aerated. Generally, the positive effect of removing air from the fluid is clearer in part-load operations, while at the highest flow

rates, the standard performance and de-aerated one are not distinguishable. The greatest increase in efficiency due to air removal is detected, where the higher performance drop was obtained in the standard condition, i.e., a test at 2900 rpm. In this condition, +8% was obtained close to the water's best efficiency point ($q^* = 1$). Solid content strongly influences standard performance. Contrary to what was found in standard conditions, the de-aerated test reported a pump head that seems to be unaffected by solid concentration. In fact, the resulting heads with 35 wt.% and 40 wt.% slurries are almost identical (Figure 10). Shaft power is not as affected as the pump head after air removal. Slight power increments, up to +3% and +8%, are found in high-speed (2900 rpm) and low-speed (2000 rpm) testing, respectively, for most part-load operations. This behavior is attributed to the lower air content in the mixture, which leads to the increase in power required to transfer energy to a greater quantity of fluid. Also for shaft power, comparing the standard test with the de-aerated one, the higher performance gap is found with the highest concentration mixture (40 wt.%). Therefore, different air content in the same fluid corresponds to different behavior only at low flow rates, when instabilities arise due to the presence of gas-locking effects. In light of this, higher kaolin concentrations promote greater air trapping and increase bubble stability. Consequently, more benefits are found in removing air from the slurry.

5. Conclusions

In this work, an experimental campaign with a small commercial centrifugal pump handling kaolin slurries is carried out to investigate the pump performance impairment due to the effect of entrained gas in NNF. Two kaolin slurries of 35 wt.% and 40 wt.% of solid concentration are tested at design speed (2900 rpm) and at two reduced speeds (2500 and 2000 rpm). Pump performance with NNF in the standard condition, i.e., in conditions similar to an industrial process, are analyzed to outline performance modifications and the instability phenomena that can arise related to fluid rheology. The impact of gaseous fraction in pump performance is then investigated by carrying out tests in the "de-aerated" condition, i.e., with reduced air content, and the main results can be summarized as follows:

- Gas-locking effects prove to occur in processing shear-thinning fluids, impairing pump performance especially in part-load operations. Tests in de-aerated conditions allow to recover up to 20% of water performance in part-load operations, while at higher flow rates, the effect of gas entrainment is substantially negligible.
- The extent of the pump operating range affected by gas-locking effect increases with the solid content in the mixture, proving that the local effective viscosity inside the machine is intimately correlated with the severity of the gas blockage.
- Pump efficiency increases up to 8% in design conditions (2900 rpm) after having reduced the air content in the mixture. When reducing pump speed, efficiency recovery slows down up to +2% at 2000 rpm.
- Pump shaft power increases almost up to 50% processing kaolin slurries, and it seems to be less affected by the presence of entrained gas in the mixture. The air removal process leads to an average shaft power increment of 5% compared to the test in the standard condition.

It appears clear that processing non-Newtonian fluids with centrifugal pumps could involve severe performance drops that must be considered during the selection process to avoid safety risks and not harm the plant's reliability. Such drops prove to be related to possible trapped gas, revealing the necessity to study the interaction between non-Newtonian fluid and the gas phase in the machining process. The study of the pump performance processing non-Newtonian fluids requires the adoption of a multidisciplinary approach capable of combining knowledge in the field of turbomachinery with the science

of material deformation theories (continuum mechanics). The outcomes of this work show how future design and performance prediction methods have to take into account the fluid characteristics (rheology, solid content, etc.) and the presence of gas-locking phenomena, thus approaching the problem of the treated fluid in a different way. The study of the process of non-Newtonian fluids must therefore be approached by including a possible fraction of gas, moving a historically single-phase/two-phase (solid–liquid) problem to a three-phase problem (solid–liquid–gas). In this light, the results could also be useful for future validation of numerical models that take into account the impairment due to the gas fraction in part-load operations.

Author Contributions: Conceptualization, A.S., N.Z. and M.P. (Michele Pinelli); methodology, A.S.; Experimental investigation, N.Z.; writing, original draft preparation and visualization, N.Z. and M.P. (Mattia Piovan). All authors have read and agreed to the published version of the manuscript.

Funding: This research received no external funding.

Data Availability Statement: The original contributions presented in this study are included in the article. Further inquiries can be directed to the corresponding author.

Acknowledgments: The authors whish to thank Valentina Mazzanti and Francesco Mollica for their support in carrying out the rheology characterization of the kaolin slurries, and Annalisa Fortini for the kaolin powder analysis with the SEM.

Conflicts of Interest: The authors declare no conflicts of interest.

Abbreviations

The following abbreviations are used in this manuscript:

BEP	Best efficiency point
C	Mechanical torque [Nm]
C_w	Weight concentration [%]
D_{imp}	Impeller diameter [mm]
d_p	Particle mean diameter [μm]
g	Gravitational acceleration [m s^{-2}]
H	Pump head [m]
h^*	Dimensionless pump head [-]
K	Consistency index [Pa s^n]
N	Rotational speed [rpm]
n	Flow index [-]
n_q	Pump specific speed [rpm $m^{0.75}$ $s^{-0.5}$]
NNF	Non-Newtonian fluid
P_s	Shaft power [W]
p	Static pressure [Pa]
Q	Volumetric flow rate [m^3 s^{-1}]
q^*	Dimensionless flow rate [-]
R_a	Average surface roughness [μm]
SEM	Scanning electron microscope
v	Fluid velocity [m s^{-1}]
$wt.\%$	Percentage by weight [%]
Z	Number of blades
z	Height [m]
Ω	Angular speed [rad s^{-1}]
ρ_s	Solid particle density [kg m^{-3}]
τ_0	Yield stress [Pa]
τ	Shear stress [Pa]

Φ	Flow coefficient [-]
Ψ	Head coefficient [-]

References

1. Gülich, J.F. *Centrifugal Pumps*; Springer: Berlin/Heidelberg, Germany, 2010.
2. Praetorius, S.; Schößer, B. *Bentonite Handbook: Lubrication for Pipe Jacking*; John Wiley & Sons: Hoboken, NJ, USA, 2017.
3. Wilson, K.C.; Addie, G.R.; Sellgren, A.; Clift, R. *Centrifugal Pumps*; Springer: Berlin/Heidelberg, Germany, 2006.
4. Abulnaga, B. *Slurry Systems Handbook*; McGraw-Hill Education: New York, NY, USA, 2021.
5. Walker, C.; Goulas, A. Performance characteristics of centrifugal pumps when handling non-newtonian homogeneous slurries. *Proc. Inst. Mech. Eng. Part A J. Power Energy* **1984**, *198*, 41–49. [CrossRef]
6. Sery, G.; Kabamba, B.; Slatter, P. Paste pumping with centrifugal pumps: Evaluation of the Hydraulic Institute chart de-rating procedures. In *Paste 2006, Proceedings of the Ninth International Seminar on Paste and Thickened Tailings, Limerick, Ireland, 3–7 April 2006* ; Australian Centre for Geomechanics: Crawley, Australia, 2006; pp. 403–412.
7. Sellgren, A.; Addie, G.; Yu, W.C. Effects of non-Newtonian mineral suspensions on the performance of centrifugal pumps. *Miner. Process. Extr. Metall. Rev.* **2000**, *20*, 239–249. [CrossRef]
8. Kalombo, J.; Haldenwang, R.; Chhabra, R.; Fester, V. Centrifugal pump derating for non-Newtonian slurries. *J. Fluids Eng.* **2014**, *136*, 679–692. [CrossRef]
9. Occari, M.; Munari, E.; Mazzanti, V.; Pinelli, M.; Mollica, F.; Suman, A. Experimental Tests with Centrifugal Pumps: Degradation of Performance, Instability and Dynamic Phenomena with Non-Newtonian Suspensions of Kaolin in Water. In Proceedings of the Fluids Engineering Division Summer Meeting, San Francisco, CA, USA, 28 July–1 August 2019; American Society of Mechanical Engineers: New York, NY, USA, 2019; Volume 59056, p. V03BT03A067.
10. Aldi, N.; Buratto, C.; Casari, N.; Dainese, D.; Mazzanti, V.; Mollica, F.; Munari, E.; Occari, M.; Pinelli, M.; Randi, S.; et al. Experimental and Numerical Analysis of a non-Newtonian Fluids processing pump. *Energy Procedia* **2017**, *126*, 762–769. [CrossRef]
11. Kabamba, B.M. Evaluation of Centrifugal Pump Performance Derating Procedures for Non-Newtonian Slurries. Ph.D. Thesis, Cape Peninsula University of Technology, Cape Town, South Africa, 2006.
12. Zanini, N.; Suman, A.; Piovan, M.; Pinelli, M. Assessment of the derating methods for centrifugal pump performance handling non-Newtonian fluids. *J. Physics Conf. Ser.* **2023**, *2648*, 012102. [CrossRef]
13. Zanini, N.; Suman, A.; Pinelli, M. Experimental test on centrifugal pump handling mining slurries. In *Turbo Expo: Power for Land, Sea, and Air*; American Society of Mechanical Engineers: New York, NY, USA, 2023; Volume 9. [CrossRef]
14. Zanini, N.; Suman, A.; Piovan, M.; Pinelli, M. Centrifugal pump performance derating with non-Newtonian slurries. In Proceedings of the Global Power and Propulsion Society, GPPS Chania24, Chania, Greece, 4–6 September 2024. [CrossRef]
15. Furlan, J.; Visintainer, R.; Sellgren, A. Pumping a 100–600 Pa yield stress clay slurry with a centrifugal pump. In *Paste 2013, Proceedings of the 16th International Seminar on Paste and Thickened Tailings, Belo Horizonte, Brazil, 17–20 June 2013*; Australian Centre for Geomechanics: Crawley, Australia, 2013; pp. 531–543.
16. Furlan, J.; Visintainer, R.; Sellgren, A. Centrifugal pump performance when handling highly non-Newtonian clays and tailings slurries. *Can. J. Chem. Eng.* **2014**, *94*, 117–130. [CrossRef]
17. Murray, H.H. Chapter 5 Kaolin Applications. In *Developments in Clay Science*; Applied Clay Mineralogy; Murray, H.H., Ed.; Elsevier: Amsterdam, The Netherlands, 2006; Volume 2, pp. 85–109. [CrossRef]
18. Teh, E.J.; Leong, Y.; Liu, Y.; Fourie, A.; Fahey, M. Differences in the rheology and surface chemistry of kaolin clay slurries: The source of the variations. *Chem. Eng. Sci.* **2009**, *64*, 3817–3825. [CrossRef]
19. Gülich, J.F. Pump Testing. In *Centrifugal Pumps*; Springer: Berlin/Heidelberg, Germany, 2020; pp. 1205–1230.
20. *ISO-9906:2012*; Rotodynamic Pumps—Hydraulic Performance Acceptance Tests—Grades 1, 2 and 3. The British Standards Institution: London, UK, 2012.
21. Leung, E.; Meah, K.; Moscola, J.; Hake, D.; Bosse, R.; Sperbeck, C.; Wickard, C.; Owrutsky, J.; Graf, K.; Acierno, R. Design of an Automated Bubble Detection Device for Neuroangiography. In Proceedings of the 21st IEEE International Conference on Environment and Electrical Engineering, Bari, Italy, 7–10 September 2021. [CrossRef]
22. Roth, H.C.; Prams, A.; Lutz, M.; Ritscher, J.; Raab, M.; Berensmeier, S. A High-Gradient Magnetic Separator for Highly Viscous Process Liquors in Industrial Biotechnology. *Chem. Eng. Technol.* **2016**, *39*, 469–476. [CrossRef]
23. Greenwood, R.; Lapčíková, B.; Surỳnek, M.; Waters, K.; Lapčík, L. The zeta potential of kaolin suspensions measured by electrophoresis and electroacoustics. *Chem. Pap.* **2007**, *61*, 83–92. [CrossRef]
24. Prasad, M.; Reid, K.; Murray, H. Kaolin: Processing, properties and applications. *Appl. Clay Sci.* **1991**, *6*, 87–119. [CrossRef]
25. Bloodworth, A.; Highley, D.E.; Mitchell, C. *Industrial Minerals Laboratory Manual: Kaolin*; British Geological Survey: Nottingham, UK, 1993.

26. Hong, E.; Herbert, C.; Yeneneh, A.; Sen, T. Rheological characteristics of mixed kaolin–sand slurry, impacts of pH, temperature, solid concentration and kaolin–sand mixing ratio. *Int. J. Environ. Sci. Technol.* **2016**, *13*, 2629–2638. [CrossRef]
27. *ISO-98-3:2008*; Uncertainty of Measurement Part 3: Guide to the Expression of Uncertainty in Measurement. International Organization for Standardization: Geneva, Switzerland, 2008.
28. *ISO-100:2008*; Evaluation of Measurement Data Guide to the Expression of Uncertainty in Measurement. International Organization for Standardization: Geneva, Switzerland, 2008.
29. Buratto, C.; Occari, M.; Aldi, N.; Casari, N.; Pinelli, M.; Spina, P.; Suman, A. Centrifugal pumps performance estimation with non-Newtonian fluids: Review and critical analysis. In Proceedings of the 12th European Conference on Turbomachinery Fluid Dynamics and Thermodynamics, ETC 2017, Stockholm, Sweden, 3–7 April 2017. [CrossRef]
30. Li, W. Effect of exit blade angle, viscosity and roughness in centrifugal pumps investigated by CFD computation. *TASK Q. Sci. Bull. Acad. Comput. Cent. Gdan.* **2011**, *15*, 21–41.
31. Paternost, G.; Bannwart, A.; Estevam, V. Experimental study of a centrifugal pump handling viscous fluid and two-phase flow. *SPE Prod. Oper.* **2015**, *30*, 146–155. [CrossRef]
32. Monte Verde, W.; Biazussi, J.L.; Sassim, N.A.; Bannwart, A.C. Experimental study of gas-liquid two-phase flow patterns within centrifugal pumps impellers. *Exp. Therm. Fluid Sci.* **2017**, *85*, 37–51. [CrossRef]
33. Gülich, J.F. Influence of the medium on performance. In *Centrifugal Pumps*; Springer: Berlin/Heidelberg, Germany, 2010; pp. 741–808.